

Communication

Conformal Titanyl Phosphate Surface Passivation for Enhancing Photocatalytic Activity

Jung Kyu Kim 

School of Chemical Engineering, Sungkyunkwan University (SKKU), Suwon 16419, Korea; legkim@skku.edu

Received: 30 July 2018; Accepted: 17 August 2018; Published: 19 August 2018



Abstract: A conformal titanyl phosphate passivation with the thickness of ca. 5 nm on the surface of TiO₂ nanoparticles for enhancing the photocatalytic degradation of organic pollutants and hydrogen production is described. The phosphate anion species bound to the surface of TiO₂ promote the favorable kinetics of photocatalytic activity and influence the catalytic reaction pathway. By using a facile surfactant-assisted sol-gel process, the surface defects of TiO₂ associated with deep traps was reduced and passivated by the phosphate anion species to form the titanyl phosphate. The strong bonds between the titanyl phosphate shell and TiO₂ core provided a long-term photochemical stability in aqueous electrolytes with enhanced photocatalytic activities. The titanyl phosphate contributed to the production and stabilization of hydroxyl radicals on the surface of photocatalyst, which facilitated the efficient photooxidation of the organic pollutants. Further, enhancing the photocatalytic hydrogen production was achieved by the titanyl phosphate modified TiO₂ (TP-TiO₂). Consequently, the conformal titanyl phosphate passivation enhanced photocatalytic activity of TiO₂. Comparing to the bare TiO₂ nanoparticles, approximately two-fold higher photocatalytic H₂ production rate was achieved by the TP-TiO₂.

Keywords: titanyl phosphate; passivation of defects; stability; hydrogen production; photodegradation of pollutant

1. Introduction

Titanium dioxide (TiO₂) is the most extensively studied metal oxide semiconductor used for diverse solar energy conversions including photovoltaics, photodegradation of organic pollutants, and photocatalytic hydrogen production [1–11]. As for the promising heterogeneous photocatalyst, numerous efforts have been conducted to enhance the photocatalytic activity of TiO₂ nanoparticles by modifying their surface properties [12]. Despite numerous advantages of TiO₂, the tremendous intrinsic defect states in TiO₂ can deteriorate the charge transfer performance of photocatalysis. The deeply localized defects in TiO₂ can act as undesired charge trap centers and promote the rapid charge recombination [13–15]. These defect states and deep traps induce the crucial charge losses [16,17].

In recent years, numerous efforts have been conducted to enhance the photocatalytic activity of TiO₂ nanoparticles by modifying their surface properties with phosphate anion (PO₄³⁻) [18–22]. The surface modification using the phosphate species can generate the negative electrostatic field at the interface. This preferred surface electrostatic field facilitates the efficient charge separation and prolongs the photo-induced charge migration [20,22]. In addition, the negative electrostatic field can activate the formation of hydrogen bonds between phosphate anions and water molecules. Thereby, the phosphate species bound on TiO₂ can promote the generation of hydroxyl radicals, resulting in the highly efficient photocatalytic degradation of organic pollutants [23]. However, the photochemical conversion efficiency can be weakened since the direct hole oxidation pathway can be hindered by the hydroxyl radicals. The adsorbed phosphate anion on the surface of TiO₂ also can increase the

resistance of electron transfer at the interface [24,25]. Therefore, a rational design of the phosphate modification is strongly required for efficient TiO₂ photocatalysis.

In this study, the TiO₂ nanoparticles were conformally modified by the titanyl phosphate passivation layer with a thickness of ca. 5 nm. The use of a facile surfactant-assisted sol-gel process with titanium isopropoxide, phosphoric acid, and polyethylene glycol as a surfactant facilitated the formation of titanyl phosphate because the phosphate anion can strongly bind the surface Ti atom with the oxygen bridge, inducing the Ti-O-P-O bonds [26]. The titanyl phosphate passivated the surface defects in TiO₂ and reduced the deep traps associated with Ti³⁺. Consequently, the titanyl phosphate modified TiO₂ (TP-TiO₂) shows significantly enhanced photocatalytic activities through the photocatalytic degradation of organic pollutant (rhodamine B) and hydrogen production experiments.

2. Materials and Methods

2.1. Material Synthesis

The facile surfactant assisted sol-gel process was conducted by using titanium(IV) isopropoxide (TTIP, 97%, Aldrich), polyethylene glycol (PEG, M_n 300, Aldrich), phosphoric acid (85 wt%, Aldrich) and methyl alcohol (anhydrous, Aldrich). The titanium precursor solution with concentration of 0.35 M was prepared by dropping the TTIP in the methyl alcohol solvent slowly (with the rate of 1 μL/s) during the vigorous stirring over 600 rpm. After fully dissolving, 3.5 M PEG was immediately injected in the precursor. Then, 0.1 M phosphoric acid was mixed with the solution. The thermal annealing process at 750 °C for 2 h was carried out to obtain the TP-TiO₂. For the bare TiO₂, the same experimental protocol was utilized without the phosphoric acid.

2.2. Material Characterization

The particle morphologies were confirmed by X-ray diffraction (XRD) by using Siemens diffractometer D500/5000 in Bragg-Brentano geometry under Cu Kα radiation and scanning electron microscopy (SEM) by using JSM-7000F. High resolution-transmission electron microscopy (HR-TEM) images and elemental mapping images were obtained from a JEOL (JEM-2100F, Japan) electron microscope with an energy dispersive spectrometer (EDS). XPS characterization was performed with ESCA2000 from VG Microtech.

2.3. Photocatalytic Activity

Photocatalytic degradation of organic pollutant was demonstrated by using 0.01 M rhodamine B (Rh. B) aqueous solution. After achieving adsorption/desorption equilibrium (by keeping the 0.05% TiO₂ solution for 2 h in dark), 1 sun (AM 1.5G 100 mW/cm²) irradiation was employed. During the light irradiation and vigorous stirring with 600 rpm, we extracted 1 mL of sample solution at each interval. After centrifuging the solutions, the concentration changes of supernatant were characterized by using a UV-VIS-NIR Spectrophotometer (UV-3600, SHIMADZU).

Photocatalytic hydrogen production was performed in a 100 mL Quartz reactor, of which openings were sealed with the silicon rubber septum. 100 mg of catalyst was dispersed in 50 mL of 1 M KHCO₃ solution. During the 1 sun (AM 1.5G 100 mW/cm²) irradiation, the suspension solution was stirred continuously. To analyze the H₂ production, we extracted 1 mL of gas from the reactor by using a glass syringe and injected the collected gas in a gas chromatography (7890A GC system, Agilent Technologies, Santa Clara, USA). Here, Ar gas was exploited as a carrier gas. The extraction and injection of generated gas were repeated at intervals.

In this study, a solar simulator (PEC-L01, PECCELL, Yokohama, Japan) was utilized as the light source. AM 1.5G filter was exploited for the 1 sun illumination with the full spectrum (350–1100 nm). The light intensity was calibrated by using a silicon reference cell (Fraunhofer ISE, Certificate No. CISE269).

2.4. Photoelectrochemical Measurement

The current density to potential (J - V) curves were obtained via the linear sweep voltammetry (LSV) mode using the three electrodes system with the standard calomel electrode as the reference electrode, Pt foil as the counter electrode and the working electrode. The measurement was carried out using a potentiostat (CHI 705E, CH Instruments, Austin, TX, USA). 1 M KHCO_3 aqueous solution was utilized as the electrolyte. The solar simulator (PEC-L01, PECCELL) was also utilized as the light source. The working electrode was prepared by the following manner [27]: 3 wt% of solution was prepared by dispersing the photocatalyst powders in 1 mL of ethanol solvent. After adding 0.5 mL of ethyl cellulose solution (10 wt% aq.), the vigorous stirring was conducted for 8 h at 80 °C. Then, 0.16 mL of α -terpineol was added. To make a paste, the stirring process was continued for 16 h more. The doctor blade method was used to coat the paste uniformly on the pre-cleaned FTO glass. Then, the annealing process was conducted at 500 °C for 30 min.

3. Results and Discussion

3.1. Morphology Characterization

The importance of crystallinity in the metal oxide photocatalysts has been widely studied. The photochemical energy conversion efficiency can be determined by their crystallinity [28,29]. In the XRD patterns (Figure 1a), the crystalline TiO_2 in anatase/rutile mixed crystalline phase (JCPDS# 21-1272 for anatase, JCPDS# 21-1276 for rutile) was observed for bare TiO_2 nanoparticles. Considering the phase transition behavior of TiO_2 , [30] the annealing process at 750 °C resulted in the anatase/rutile mixed crystalline phase. However, the rutile phase peaks were diminished in TP- TiO_2 while the anatase phase and strong titanyl phosphate (JCPDS# 35-802) peaks were observed, even the same annealing process was conducted at 750 °C for TP- TiO_2 . The suppressed phase transformation between anatase and rutile is attributed to the phosphate anions, of which good affinity to Ti atoms hindered the phase transformation of TiO_2 [31]. Even the phosphate anions induced these significant changes in crystallinity, no significant changes in morphology were not characterized in SEM images (Figure 1b and c). However, a slight increase in the size of overall particles was observed in TP- TiO_2 . The estimated particle size was *avg.* 51 nm (\pm 27) for bare TiO_2 and *avg.* 58 nm (\pm 18) for TP- TiO_2 . This presumably resulted from the phosphate anions. HR-TEM images of TP- TiO_2 (Figure 1d and e) demonstrate that the surface of TP- TiO_2 was conformally passivated by the titanyl phosphate layer of which thickness was ca. 5 nm. The fringe pattern in Figure 1e and the reduced fast Fourier transform (FFT) pattern in the insert image indicate that the core TiO_2 is composed of the anatase phase. The anatase (101) was clearly defined by the distinct lattice space of 0.35 nm. For further determination of this TiO_2 -core @ titanyl phosphate-shell structure, the elemental mapping of Ti, O, and P atoms was performed using TEM-EDS (Figure 1f). As shown in the high angle annular dark field scanning (HAADF) TEM image, the mapping was focused on the surface passivation layer. This elemental mapping image shows that all elements (Ti, O and P atoms) are well dispersed in the passivation layer, which implies that the surface of TP- TiO_2 is conformally passivated by titanyl phosphate.

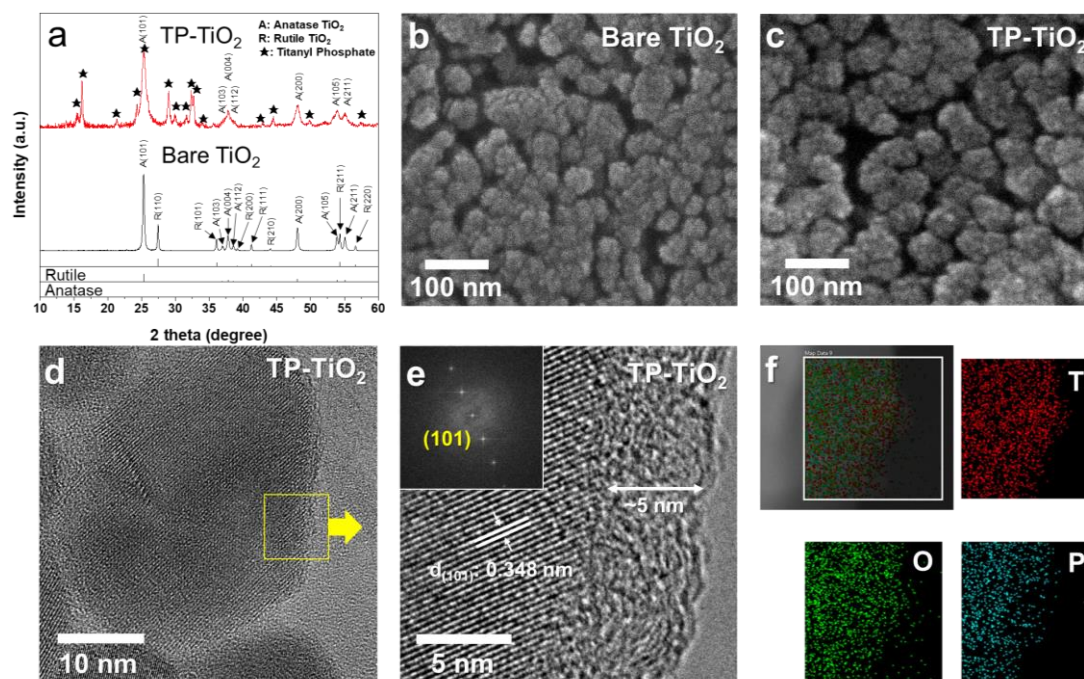


Figure 1. (a) XRD pattern of bare and TP-TiO₂. SEM images of bare (a) and TP-TiO₂ (b). (d) and (e) HR-TEM images of TP-TiO₂. The inserted image is a reduced FFT pattern. (f) HAADF TEM image and EDS elemental mapping of Ti, O and P atoms for TP-TiO₂.

3.2. Chemical Modification

For the sake of understanding the chemical modification, XPS characterization was performed as shown in Figure 2. The C 1s XPS spectra of bare and TP-TiO₂ were utilized to reference the measured XPS results, where the binding energy of major C-C peaks are 284.8 eV (Supplementary Figure S1). The positive shift of Ti 2p_{1/2} and Ti 2p_{3/2} peaks of TP-TiO₂ were observed in the Ti 2p XPS spectra (Figure 2a). The shift in Ti 2p can be attributed to the ameliorated surface states [32,33]. This positive shift of Ti 2p demonstrates that the Ti-O-P-O bonds were successfully formed on the surface of the TiO₂ core particle, and resulted in the reduction of trap states originated from Ti³⁺ defects. The O 1p XPS spectra are displayed in Figure 2b. Two dominant peaks of bare TiO₂ at 530.1 and 531.6 eV are assigned to the lattice oxygen (O_L) and surface oxygen (O_S), respectively. Here, the lattice oxygen indicates Ti-O-Ti chain. However, the TP-TiO₂ exhibited four peaks at 530.1, 531.1, 531.6, and 532.9 eV. The newly arising peak at 531.1 eV, corresponding to Ti-O-P bond, demonstrates the formation of titanyl phosphate on the surface of TiO₂ [34]. Moreover, the sharper O_S peak centered at 531.6 eV is also attributed to the OH species or O vacancies that originated from the titanyl phosphate groups [35]. Considering the disordered structure of surface titanyl phosphate layer in the TEM image (Figure 2e), the phosphate anion groups can induce -OH groups or O vacancies on TP-TiO₂. In addition, the shoulder peak at 532.9 eV, can be attributed to chemisorbed oxygen species (O_C) such as CO₂ or H₂O [36]. During the sol-gel process, the structure determining agent (i.e. PEG) can be bounded to the phosphate anion species via hydrogen bonding. Therefore, the carbon or oxygen related species (including CO₂ or carboxylic groups) can be remained on the surface of TP-TiO₂ after performing the annealing process. As shown in C 1s XPS (Figure S1), the slight increase in C-O (ca. 286.5 eV) and C=O (ca. 288.5 eV) peaks were observed in TP-TiO₂, which implies that the oxygen species can be adsorbed onto TP-TiO₂ [7]. P 2p XPS is shown in Figure 2c, where TP-TiO₂ has two sharp peaks at 133.0 and 133.9 eV corresponding to P 2p_{3/2} and P 2p_{1/2}, respectively. These peaks can be assigned to the monodentate coordinated phosphate anion (PO₄³⁻), when it comes to the binding energies of Na₂HPO₄ (133.1 eV) and NaH₂PO₄ (133.9 eV) [23]. Additional T-P bond was not observed in the XPS spectrum.

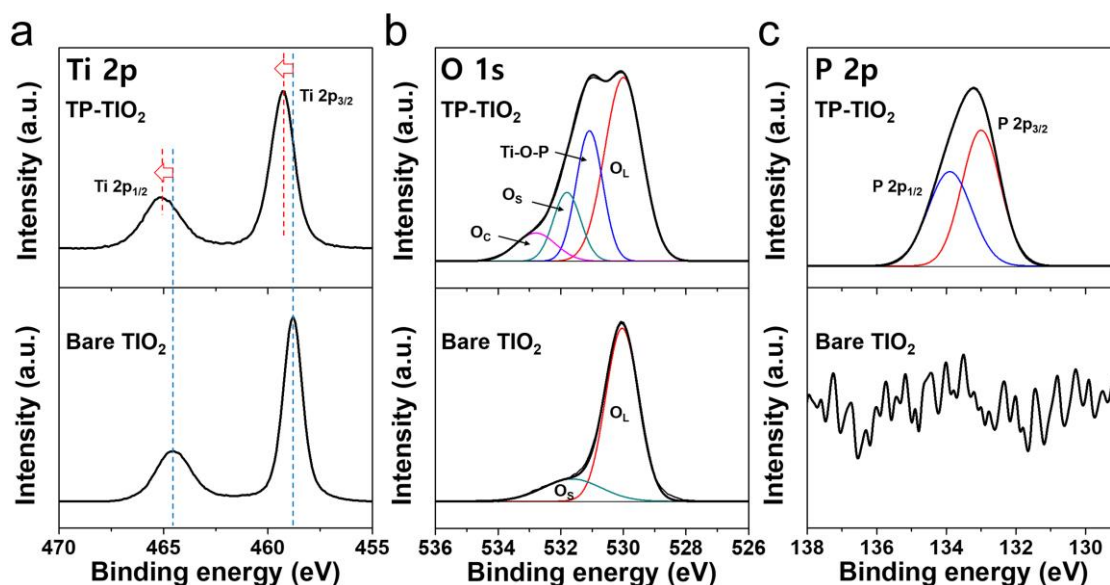


Figure 2. (a) Ti 2p; (b) O 1s; and (c) P 2p XPS spectra of bare and TP-TiO₂.

3.3. Photocatalytic Performance

The photocatalytic activity was investigated via the photodegradation experiment using rhodamine B aqueous solution. In Figure 3a, TP-TiO₂ shows outstanding photocatalytic activity comparing to bare TiO₂. In order to calculate their rate constants, natural logarithmic plots were prepared as shown in Figure 3b. By using the first order reaction rate equation ($C/C_0 = \exp(-kt)$), the rate constants (k) are calculated [27]. TP-TiO₂ shows approximately 3-folds higher k value than bare TiO₂. Furthermore, Figure 3c shows the performances of photocatalytic hydrogen production. Since the surface phosphate groups can promote the formation of hydroxyl radicals in water, 1 M KHCO₃ aqueous solution was exploited as the electrolyte to stabilize the H₂O₂ production and induce the 2-electron pathway for water splitting [23,37–40]. Significantly higher photocatalytic hydrogen production rate ($86.7 \mu\text{mol h}^{-1}\text{g}^{-1}$ for TP-TiO₂ and $46.1 \mu\text{mol h}^{-1}\text{g}^{-1}$ for bare TiO₂) was achieved. Moreover, TP-TiO₂ also shows much stable photocatalytic activity than bare TiO₂ due to the conformal passivation of titanyl phosphate. After continuous operation for 24 h, negligible changes in the production rate was observed in TP-TiO₂, whereas visible changes were shown by bare TiO₂. TEM image of TP-TiO₂ after 24 h of operation (Supplementary Figure S2) shows the long-term stability of titanyl phosphate layer. The surface modification using the phosphate species can generate the negative electrostatic field, which facilitates the efficient charge migration. The negative electrostatic field also can activate the formation of hydrogen bond between phosphate anion and water molecule. This promotes the adsorption of water molecules at the surface of photocatalysts and the generation of hydroxyl radical, resulting in high efficient photocatalytic properties [20,22,23]. Moreover, the charge recombination was suppressed since the charge trap states of TiO₂ were ameliorated by the surface titanyl phosphate passivation layer. It is noteworthy that no significant changes in the UV-Vis absorbance spectra were observed (Supplementary Figure S3). This implies that the surface passivation layer with the disordered structure does not influence the light harvesting property of photocatalyst [41]. To investigate the efficient charge migration properties, the photoelectrochemical (PEC) response was characterized using the three electrodes system, of which working electrode was comprised of the TiO₂ photocatalysts (Supplementary Figure S4). 1 M KHCO₃ aqueous solution (pH 7.4) was also used as the electrolyte. The significantly enhanced photocurrent density value of TP-TiO₂ was resulted from not only the modified surface catalytic kinetics, but also the suppressed charge recombination and promoted charge migration [41]. Additionally, the external quantum

efficiency (EQE) spectra were investigated to demonstrate the enhanced performance of TP-TiO₂ in Supplementary Figure S4b.

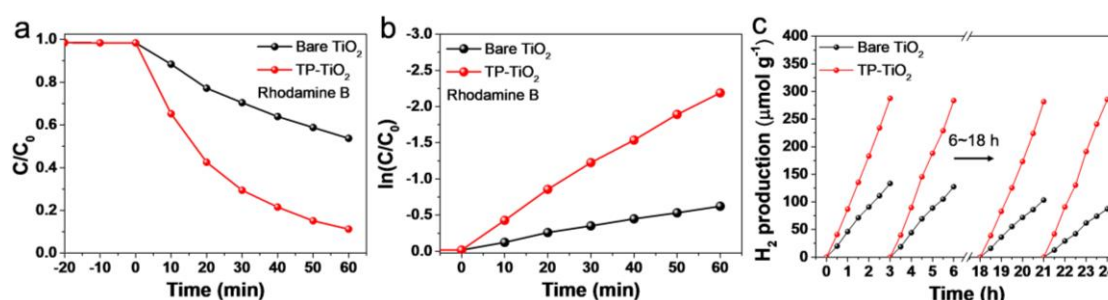


Figure 3. (a) Concentration changes in rhodamine B aqueous solution by photodegradation; (b) Natural logarithmic plots for the study of the kinetics of rhodamine B photodegradation profiles; (c) Photocatalytic hydrogen production and cycling performance during 24 h of continuous reaction in the presence of 1 M KHCO₃.

4. Conclusions

The TiO₂ photocatalysts were conformally modified by the titanyl phosphate passivation layer with a thickness of ca. 5 nm. The use of a facile surfactant-assisted sol-gel process facilitated the formation of titanyl phosphate on the surface of TiO₂ nanoparticles. The phosphate anions are strongly bound onto the surface Ti atoms with oxygen bridges, inducing the Ti-O-P-O bonds. Thereby, the surface titanyl phosphate bonds resulted in the reduction of trap states originated from Ti³⁺ defects. These strong bonds enable the long-term photochemical performance in liquid electrolytes with enhanced photocatalytic activities. Moreover, the titanyl phosphate contributed to the production and stabilization of hydroxyl radicals on the surface of TiO₂ nanoparticles, which facilitated the efficient photooxidation of the organic pollutants. Furthermore, the significantly enhanced photocatalytic hydrogen production performance was observed by the titanyl phosphate modified TiO₂. Consequently, high photocatalytic activity was achieved by introducing the titanyl phosphate surface passivation layer. The demonstrated titanyl phosphate modification enables the conformal passivation of TiO₂ photocatalysts with tunable properties, which is conducive to diverse photochemical conversion applications.

Supplementary Materials: The following are available online at <http://www.mdpi.com/2076-3417/8/8/1402/s1>, Figure S1: C 1s XPS spectra of bare and TP-TiO₂, Figure S2: TEM image of TP-TiO₂ after carrying out the photocatalytic H₂ production experiment for 24 hours, Figure S3: UV-Vis absorbance spectra and Tauc plot (insert) of bare and TP-TiO₂, Figure S4: Current density to potential (*J*-*V*) curves, EQE and IQE spectra of bare and TP-TiO₂ under on/off chopped 1 sun irradiation.

Acknowledgments: The authors acknowledge the support of the NRF of Korea (NRF-2018R1D1A1B07050875).

Conflicts of Interest: The authors declare no conflict of interest.

References

1. Fujishima, A.; Honda, K. Electrochemical photolysis of water at a semiconductor electrode. *Nature* **1972**, *238*, 37–38. [[CrossRef](#)] [[PubMed](#)]
2. O'Regan, B.; Grätzel, M. A low-cost, high-efficiency solar cell based on dye-sensitized colloidal TiO₂ films. *Nature* **1991**, *353*, 737–740. [[CrossRef](#)]
3. Bard, A.J. Photoelectrochemistry. *Science* **1980**, *207*, 139–144. [[CrossRef](#)] [[PubMed](#)]
4. Kim, J.K.; Jang, J.-r.; Choi, N.; Hong, D.; Nam, C.-H.; Yoo, P.J.; Park, J.H.; Choe, W.-S. Lysozyme-mediated biomineralization of titanium–tungsten oxide hybrid nanoparticles with high photocatalytic activity. *Chem. Commun.* **2014**, *50*, 12392–12395. [[CrossRef](#)] [[PubMed](#)]

5. Crossland, E.J.W.; Noel, N.; Sivaram, V.; Leijtens, T.; Alexander-Webber, J.A.; Snaith, H.J. Mesoporous TiO₂ single crystals delivering enhanced mobility and optoelectronic device performance. *Nature* **2013**, *495*, 215–219. [[CrossRef](#)] [[PubMed](#)]
6. Giordano, F.; Abate, A.; Baena, J.P.C.; Saliba, M.; Matsui, T.; Im, S.H.; Zakeeruddin, S.M.; Nazeeruddin, M.K.; Hagfeldt, A.; Graetzel, M. Enhanced electronic properties in mesoporous TiO₂ via lithium doping for high-efficiency perovskite solar cells. *Nat. Commun.* **2016**, *7*. [[CrossRef](#)] [[PubMed](#)]
7. Kim, J.K.; Chai, S.U.; Cho, Y.; Cai, L.L.; Kim, S.J.; Park, S.; Park, J.H.; Zheng, X.L. Ultrafast flame annealing of TiO₂ paste for fabricating dye-sensitized and perovskite solar cells with enhanced efficiency. *Small* **2017**, *13*. [[CrossRef](#)] [[PubMed](#)]
8. Kim, J.K.; Shin, K.; Cho, S.M.; Lee, T.W.; Park, J.H. Synthesis of transparent mesoporous tungsten trioxide films with enhanced photoelectrochemical response: Application to unassisted solar water splitting. *Energy Environ. Sci.* **2011**, *4*, 1465–1470. [[CrossRef](#)]
9. Onotri, L.; Race, M.; Clarizia, L.; Guida, M.; Alfè, M.; Andreozzi, R.; Marotta, R. Solar photocatalytic processes for treatment of soil washing wastewater. *Chem. Eng. J.* **2017**, *318*, 10–18. [[CrossRef](#)]
10. Malato, S.; Blanco, J.; Vidal, A.; Alarcón, D.; Maldonado, M.I.; Cáceres, J.; Gernjak, W. Applied studies in solar photocatalytic detoxification: An overview. *Sol. Energy* **2003**, *75*, 329–336. [[CrossRef](#)]
11. Aguirre, M.E.; Zhou, R.; Eugene, A.J.; Guzman, M.I.; Grela, M.A. Cu₂O/TiO₂ heterostructures for CO₂ reduction through a direct Z-scheme: Protecting Cu₂O from photocorrosion. *Appl. Catal. B: Environ.* **2017**, *217*, 485–493. [[CrossRef](#)]
12. Park, H.; Park, Y.; Kim, W.; Choi, W. Surface modification of TiO₂ photocatalyst for environmental applications. *J. Photochem. Photobio. C: Photochem. Rev.* **2013**, *15*, 1–20. [[CrossRef](#)]
13. Naldoni, A.; Allieta, M.; Santangelo, S.; Marelli, M.; Fabbri, F.; Cappelli, S.; Bianchi, C.L.; Psaro, R.; Dal Santo, V. Effect of nature and location of defects on bandgap narrowing in black TiO₂ nanoparticles. *J. Am. Chem. Soc.* **2012**, *134*, 7600–7603. [[CrossRef](#)] [[PubMed](#)]
14. Liu, G.; Yin, L.C.; Wang, J.Q.; Niu, P.; Zhen, C.; Xie, Y.P.; Cheng, H.M. A red anatase TiO₂ photocatalyst for solar energy conversion. *Energy Environ. Sci.* **2012**, *5*, 9603–9610. [[CrossRef](#)]
15. Li, Y.G.; Zhu, L.P.; Guo, Y.M.; Song, H.; Lou, Z.R.; Ye, Z.Z. A new type of hybrid nanostructure: Complete photo-generated carrier separation and ultrahigh photocatalytic activity. *J. Mater. Chem. A* **2014**, *2*, 14245–14250. [[CrossRef](#)]
16. Gao, L.; Li, Y.; Ren, J.; Wang, S.; Wang, R.; Fu, G.; Hu, Y. Passivation of defect states in anatase TiO₂ hollow spheres with mg doping: Realizing efficient photocatalytic overall water splitting. *Appl. Catal. B: Environ.* **2017**, *202*, 127–133. [[CrossRef](#)]
17. Tong, H.; Ouyang, S.X.; Bi, Y.P.; Umezawa, N.; Oshikiri, M.; Ye, J.H. Nano-photocatalytic materials: Possibilities and challenges. *Adv. Mater.* **2012**, *24*, 229–251. [[CrossRef](#)] [[PubMed](#)]
18. Minero, C.; Mariella, G.; Maurino, V.; Pelizzetti, E. Photocatalytic transformation of organic compounds in the presence of inorganic anions. 1. Hydroxyl-Mediated and Direct Electron-Transfer reactions of Phenol on a Titanium Dioxide–Fluoride system. *Langmuir* **2000**, *16*, 2632–2641. [[CrossRef](#)]
19. Körösi, L.; Papp, S.; Bertóti, I.; Dékány, I. Surface and bulk composition, structure, and photocatalytic activity of phosphate-modified TiO₂. *Chem. Mater.* **2007**, *19*, 4811–4819. [[CrossRef](#)]
20. He, T.; Weng, Y.; Yu, P.; Liu, C.; Lu, H.; Sun, Y.; Zhang, S.; Yang, X.; Liu, G. Bio-template mediated in situ phosphate transfer to hierarchically porous TiO₂ with localized phosphate distribution and enhanced photoactivities. *J. Phys. Chem. C* **2014**, *118*, 4607–4617. [[CrossRef](#)]
21. Shao, G.-S.; Wang, F.-Y.; Ren, T.-Z.; Liu, Y.; Yuan, Z.-Y. Hierarchical mesoporous phosphorus and nitrogen doped titania materials: Synthesis, characterization and visible-light photocatalytic activity. *Appl. Catal. B: Environ.* **2009**, *92*, 61–67. [[CrossRef](#)]
22. Jing, L.; Zhou, J.; Durrant, J.R.; Tang, J.; Liu, D.; Fu, H. Dynamics of photogenerated charges in the phosphate modified TiO₂ and the enhanced activity for photoelectrochemical water splitting. *Energy Environ. Sci.* **2012**, *5*, 6552–6558. [[CrossRef](#)]
23. Zhao, D.; Chen, C.C.; Wang, Y.F.; Ji, H.W.; Ma, W.H.; Zang, L.; Zhao, J.C. Surface modification of TiO₂ by phosphate: Effect on photocatalytic activity and mechanism implication. *J. Phys. Chem. C* **2008**, *112*, 5993–6001. [[CrossRef](#)]

24. Yu, J.C.; Zhang, L.Z.; Zheng, Z.; Zhao, J.C. Synthesis and characterization of phosphated mesoporous titanium dioxide with high photocatalytic activity. *Chem. Mater.* **2003**, *15*, 2280–2286. [[CrossRef](#)]
25. Ortiz-Islas, E.; Gomez, R.; Lopez, T.; Navarrete, J.; Aguilar, D.H.; Quintana, P. Effect of the crystallite size in the structural and textural properties of sulfated and phosphated titania. *Appl. Surf. Sci.* **2005**, *252*, 807–812. [[CrossRef](#)]
26. Connor, P.A.; McQuillan, A.J. Phosphate adsorption onto TiO₂ from aqueous solutions: An in situ internal reflection infrared spectroscopic study. *Langmuir* **1999**, *15*, 2916–2921. [[CrossRef](#)]
27. Kim, J.K.; Bae, S.; Kim, W.; Jeong, M.J.; Lee, S.H.; Lee, C.-L.; Choi, W.K.; Hwang, J.Y.; Park, J.H.; Son, D.I. Nano carbon conformal coating strategy for enhanced photoelectrochemical responses and long-term stability of ZnO quantum dots. *Nano Energy* **2015**, *13*, 258–266. [[CrossRef](#)]
28. Linsebigler, A.L.; Lu, G.Q.; Yates, J.T. Photocatalysis on TiO₂ surfaces—principles, mechanisms, and selected results. *Chem. Rev.* **1995**, *95*, 735–758. [[CrossRef](#)]
29. Zhang, Y.Y.; Chen, J.Z.; Li, X.J. Preparation and photocatalytic performance of anatase/rutile mixed-phase TiO₂ nanotubes. *Catal. Lett.* **2010**, *139*, 129–133. [[CrossRef](#)]
30. Nolan, N.T.; Seery, M.K.; Pillai, S.C. Spectroscopic investigation of the anatase-to-rutile transformation of sol-gel-synthesized TiO₂ photocatalysts. *J. Phys. Chem. C* **2009**, *113*, 16151–16157. [[CrossRef](#)]
31. Antonelli, D.M.; Ying, J.C. Synthesis of hexagonally packed mesoporous TiO₂ by a modified sol-gel method. *Angew. Chem. Int. Ed.* **1995**, *34*, 2014–2017. [[CrossRef](#)]
32. Yermakov, A.Y.; Zakharova, G.S.; Uimin, M.A.; Kuznetsov, M.V.; Molochnikov, L.S.; Konev, S.F.; Konev, A.S.; Minin, A.S.; Mesilov, V.V.; Galakhov, V.R.; et al. Surface magnetism of cobalt-doped anatase TiO₂ nanopowders. *J. Phys. Chem. C* **2016**, *120*, 28857–28866. [[CrossRef](#)]
33. Jun, P.; Duong, T.; Zhou, X.Z.; Shen, H.P.; Wu, Y.L.; Mulmudi, H.K.; Wan, Y.M.; Zhong, D.Y.; Li, J.T.; Tsuzuki, T.; Weber, K.J.; et al. Efficient indium-doped Ti_x electron transport layers for high-performance perovskite solar cells and perovskite-silicon tandems. *Adv. Energy Mater.* **2017**, *7*, 1601768. [[CrossRef](#)]
34. Boukhvalov, D.W.; Korotian, D.M.; Efremov, A.V.; Kurmaev, E.Z.; Borchers, C.; Zhidkov, I.S.; Gunderov, D.V.; Valiev, D.V.; Gavrilov, N.V.; Cholakh, S.O. Modification of titanium and titanium dioxide surfaces by ion implantation: Combined XPS and DFT study. *Phys. Status Solidi B* **2015**, *252*, 748–754. [[CrossRef](#)]
35. Duan, X.; Liu, J.; Chen, Y.; Li, Z.; Zhu, P.; Jiang, H. Modification of RbTiOPO₄ (001) crystal surface induced by Ar⁺ ion bombardment: X-ray photoelectron spectroscopy and first-principles studies. *Vacuum* **2018**, *147*, 38–44. [[CrossRef](#)]
36. Zhang, X.; Qin, J.; Xue, Y.; Yu, P.; Zhang, B.; Wang, L.; Liu, R. Effect of aspect ratio and surface defects on the photocatalytic activity of ZnO nanorods. *Sci. Rep.* **2014**, *4*, 4596. [[CrossRef](#)] [[PubMed](#)]
37. Kim, J.K.; Shi, X.J.; Jeong, M.J.; Park, J.; Han, H.S.; Kim, S.H.; Guo, Y.; Heinz, T.F.; Fan, S.H.; Lee, C.L.; et al. Enhancing Mo:BiVO₄ solar water splitting with patterned Au nanospheres by plasmon-induced energy transfer. *Adv. Energy Mater.* **2018**, *8*. [[CrossRef](#)]
38. Liu, J.; Liu, Y.; Liu, N.; Han, Y.; Zhang, X.; Huang, H.; Lifshitz, Y.; Lee, S.-T.; Zhong, J.; Kang, Z. Metal-free efficient photocatalyst for stable visible water splitting via a two-electron pathway. *Science* **2015**, *347*, 970–974. [[CrossRef](#)] [[PubMed](#)]
39. Dimitrijevic, N.M.; Vijayan, B.K.; Poluektov, O.G.; Rajh, T.; Gray, K.A.; He, H.; Zapol, P. Role of water and carbonates in photocatalytic transformation of CO₂ to CH₄ on titania. *J. Am. Chem. Soc.* **2011**, *133*, 3964–3971. [[CrossRef](#)] [[PubMed](#)]
40. Pilli, S.K.; Deutsch, T.G.; Furtak, T.E.; Brown, L.D.; Turner, J.A.; Herring, A.M. BiVO₄/CuWO₄ heterojunction photoanodes for efficient solar driven water oxidation. *Phys. Chem. Chem. Phys.* **2013**, *15*, 3273–3278. [[CrossRef](#)] [[PubMed](#)]
41. Kim, J.K.; Cho, Y.; Jeong, M.J.; Levy-Wendt, B.; Shin, D.; Yi, Y.; Wang, D.H.; Zheng, X.L.; Park, J.H. Rapid formation of a disordered layer on monoclinic BiVO₄: Co-catalyst-free photoelectrochemical solar water splitting. *ChemSuschem* **2018**, *11*, 933–940. [[CrossRef](#)] [[PubMed](#)]

